Available online at www.sciencedirect.com
ScienceDirect
Applied Acoustics 69 (2008) 994–1002
applied acoustics
www.elsevier.com/locate/apacoust

Influence of atmospheric refraction on the performance of an outdoor ultrasonic pulse compression system

Fernando J. Álvarez [a,*], J. Ureña [b], A. Hernàndez [b], M. Mazo [b], J.J. García [b], A. Jiménez [b]

[a] Department of Electrical Engineering, Electronics and Automatics, University of Extremadura. 10071 Cáceres, Spain
[b] Department of Electronics, University of Alcalá, 28871 Alcalá de Henares, Madrid, Spain

Received 21 December 2006; received in revised form 13 July 2007; accepted 13 July 2007
Available online 11 September 2007

Abstract

Nowadays, many ultrasonic sensory systems are being developed to operate outdoors, where they are finding a variety of applications, such as local positioning, vehicle navigation or obstacle detection. To assure the reliable operation of these systems under any meteorological condition, it is necessary to achieve a thorough comprehension of the effects that the different atmospheric phenomena can have on the propagation of these acoustic waves. This paper deals with one of these phenomena, atmospheric refraction, and its influence on the performance of an ultrasonic system whose signals are detected by matched filtering.

Keywords: Atmospheric refraction; Ultrasonic sensory systems; Pulse compression

1. Introduction

Ultrasonic sensory systems have experienced a remarkable development in the last decade, since the signal coding and the pulse compression techniques used in radar theory were adopted by these systems. These techniques notably improve essential properties of these systems such as their spatial resolution, the time precision and the robustness to noise, what makes them very suitable for high precision tasks that have been traditionally reserved for other technologies. Furthermore, the high performance achieved in this way encourages the development of new systems intended for outdoor operation, where the classical systems based on threshold detection of the signal envelope cannot reliably operate under any meteorological condition.

However, the use of ultrasonic signals outdoors must face new problems that do not exist in more controlled environments. One of these problems is the refraction caused by sound speed dependence on height. This phenomenon brings about not only a variation in the Sound Pressure Level (SPL) of the received signals, but also can distort them as a consequence of the filtering effect associated with the emission pattern of the transducers. Needless to say, this distortion could have a dramatic effect on the performance of the pulse compression system, where the emitted signals are detected by recognition of a certain pattern.

This paper deals with the influence that atmospheric refraction can have on the performance of an ultrasonic pulse compression system designed to operate in the surface layer of the atmosphere, regardless the final application of the system, whether it be obstacle detection, ranging or local positioning.

The paper begins in Section 2 with a thorough analysis of the refraction phenomenon. Starting with the wind and temperature profiles, a simplified expression for the apparent sound speed is obtained through the linearization of these profiles in the first Fresnel ellipsoid. This expression allows us to determine the departure angle of an

* Corresponding author. Tel.: +34 927 25 71 95; fax: +34 927 25 72 03.
E-mail address: fafranco@unex.es (F.J. Álvarez).

0003-682X/$ - see front matter © 2007 Elsevier Ltd. All rights reserved.
doi:10.1016/j.apacoust.2007.07.006

ultrasonic ray received at a certain distance under particular meteorological conditions. As the calculations necessary to obtain the wind and temperature profiles from a set of meteorological parameters are many and tedious, a computation algorithm has been developed to automate this process. This algorithm is described in detail in the last part of Section 2.

Section 3 studies the effect that the previous phenomenon can have on the emission of encoded signals through ultrasonic transducers that are characterized by a particular emission pattern, and how this effect can affect the proper detection of these signals by matched filtering.

Section 4 shows some results obtained from the analysis of a real ultrasonic pulse compression system; and finally, the main conclusions of this work are outlined in Section 5.

2. Refraction of an ultrasonic beam in the surface layer of the atmosphere

2.1. Phenomenon description

Temperature and wind are the two meteorological parameters that have a stronger influence on sound speed propagation, whose apparent value s can be given as:

$$s \simeq v_{\mathrm{p}} + 331.6 \cdot \sqrt{1 + \frac{T}{273.15}}, \tag{1}$$

where v_{p} is the component of the wind in the direction of propagation and T is the temperature in Celsius. Eq. (1) is a good approximation provided the normal component of the wind v_{n} is small compared to the wave speed c [1]. In the atmosphere, both temperature and wind speed are strongly dependent on height, a dependency inherited by sound speed that causes the refraction of acoustic waves propagating outdoors.

This phenomenon can be quantitatively analyzed using the well-known Snell's law to calculate the trajectory followed by an acoustic ray:

$$\cos\theta = \frac{s(z)}{s_0}, \tag{2}$$

where θ is the angle between the acoustic ray and the horizontal plane; $s(z)$ is an expression for the apparent sound speed as a function of height and s_0 represents the propagation speed at a reference height. The expression for $s(z)$ can be obtained from (1) if the profiles for the temperature $T(z)$ and wind velocity $v(z)$ are known. In the surface layer of the atmosphere, whose height may vary from 10 m on clear nights to 100 m on strongly windy days, these profiles can be obtained from Monin–Obukhov similarity theory [2]:

$$T(z) = T(z_0) + \frac{T^*}{K_a}\left[\ln\left(\frac{z}{z_0}\right) - \psi_T\left(\frac{z}{L_{\mathrm{mo}}}\right)\right] - \frac{G_0}{c_p}(z - z_0), \tag{3a}$$

$$v_l(z) = \frac{v^*}{K_a}\left[\ln\left(\frac{z}{z_0}\right) - \psi_v\left(\frac{z}{L_{\mathrm{mo}}}\right)\right]. \tag{3b}$$

In these expressions K_a is the *Von Karman's* constant, whose value is approximately 0.4; c_p is the air specific heat at constant pressure; and G_0 is the gravitational acceleration module. Constants T^* and v^* represent two scale values for temperature and wind speed respectively and, although they have a clear physical meaning, their values are usually experimentally adjusted through (3) if one wind measurement and two temperature measurements are available at known heights. Constant z_0 is the *roughness length*, and it is a measure of the minimum height below which the profiles above are not valid. Its value depends on the roughness characteristics of the terrain and can be obtained with enough accuracy from Table 1 by simple inspection of the terrain [3].

Functions ψ_T and ψ_v appearing in the equations above depend on the type of atmosphere. These functions have been empirically adjusted to obtain the following expressions [3]:

$$\psi_T\left(\frac{z}{L_{\mathrm{mo}}}\right) = \begin{cases} 2\ln\left[\frac{1}{2}(1+x^2)\right] & \text{Unstable} \\ 0 & \text{Neutral} \\ -5\frac{z}{L_{\mathrm{mo}}} & \text{Stable} \end{cases} \tag{4a}$$

$$\psi_v\left(\frac{z}{L_{\mathrm{mo}}}\right) = \begin{cases} \ln\left[\left(\frac{1+x^2}{2}\right)\left(\frac{1+x}{2}\right)^2\right] - 2\arctan x - \frac{\pi}{2} & \text{Unstable} \\ 0 & \text{Neutral} \\ -5\frac{z}{L_{\mathrm{mo}}} & \text{Stable} \end{cases} \tag{4b}$$

being $x = (1 - 16z/L_{\mathrm{mo}})^{\frac{1}{4}}$.

Finally L_{mo} is the *Monin–Obukhov length* that depends basically on the vertical flux of heat at the surface. Since this flux cannot be easily measured experimentally, L_{mo} is not directly calculated in practice. Instead, its value is inferred from the relation of this magnitude with the roughness length and Turner classes found by Golder [4].

Turner classes constitute a classification method for different types of atmospheres, which is based on the relative importance that thermal convection and mechanical turbulence have on a particular atmosphere. There exist seven classes numbered from 1 to 7. The first three classes correspond to unstable atmospheres, where thermal convection prevails over mechanical turbulence (sunny days with weak winds), class 4 represents neutral atmospheres where thermal convection does not exist and only mechanical turbulence is present (days and nights with strong winds), and the last three classes correspond to stable atmospheres characterized by an inversion of the temperature gradient (clear

Table 1
Typical values for z_0 shown in [3]

Type of terrain	z_0 (m)
Water or ice	10^{-4}
Mown grass	10^{-2}
Long grass, rocky ground	0.05
Pasture land	0.20
Suburban housing	0.6
Forests, cities	1–5

nights with weak winds). The class a certain atmosphere belongs to, may be directly calculated from the solar altitude (that determines the intensity of the radiation received), the cloud cover, and the wind speed at a reference height. The relation experimentally obtained by Golder between z_0, L_{mo} and Turner classes is represented in Fig. 1.

2.2. Linearization of $s(z)$

As stated before, this work is focused on the influence that atmospheric refraction has on the signals emitted by an ultrasonic system that uses the air as transmission channel. These systems are characterized by a very high atmospheric absorption, since this attenuation mechanism is proportional to the squared value of the acoustic frequency, and values of some dB/m for the absorption coefficient are common in the range of frequencies between 20 kHz and 100 kHz [5]. Hence, a signal horizontally emitted can cover a maximum distance of several tens of meters before being detected, and the maximum vertical deviation caused by refraction cannot exceed a few meters even in the most unfavorable conditions. In this situation, it can be assumed as a good approximation that the apparent sound speed depends linearly on height, and thus, the trajectory followed by an acoustic ray is an arc of circumference, as shown in Fig. 2. From this figure, and taking Eq. (2) into account, the departure angle θ_s of the ray detected at a distance r from the emitter in the same horizontal plane can be easily obtained as:

$$\theta_s = \arctan\left(\frac{r \cdot g}{2 \cdot s_0}\right) \tag{5}$$

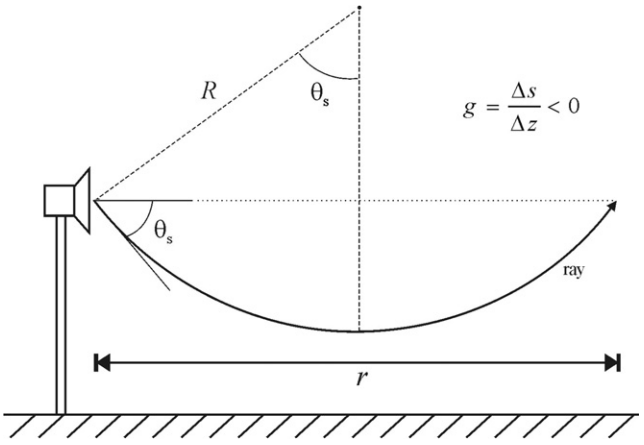

Fig. 2. Trajectory followed by an acoustic ray under a constant sound speed gradient.

where $g = \frac{ds}{dz}$ is the constant speed gradient and s_0 is the apparent sound speed at the emitter height.

The linearization method used in this work is the one proposed by L'Esperance and Daigle [6], where the constant gradient is obtained as the average sound speed variation in the first Fresnel ellipsoid. This ellipsoid is represented in Fig. 3, and it is defined as the region of the space where the differences between the length of the direct path and the length of any diffracted path is less than half wavelength:

$$r_1 + r_2 - r = \frac{\lambda}{2}. \tag{6}$$

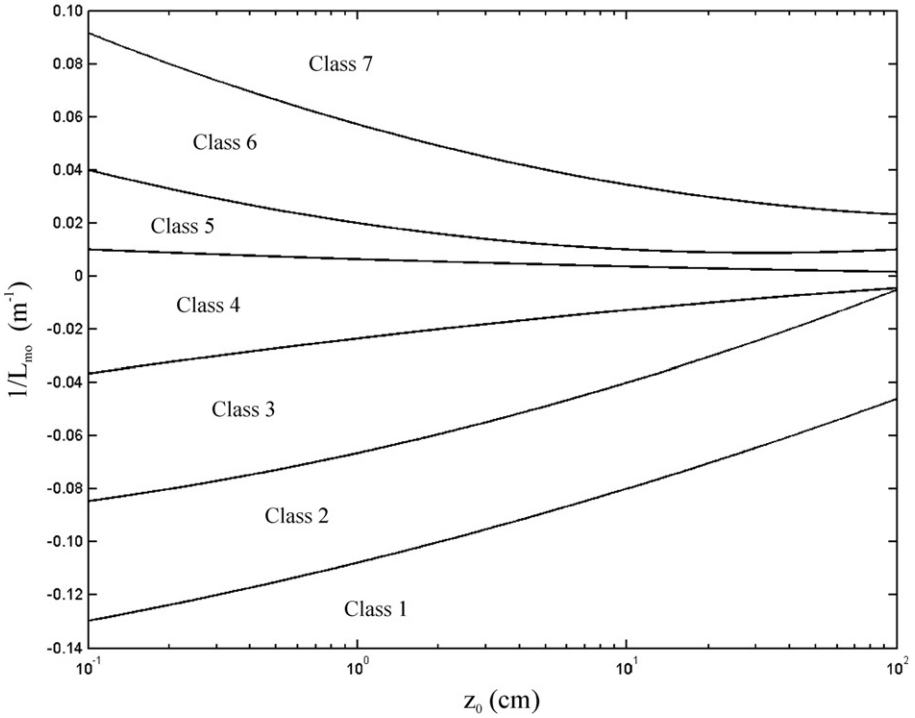

Fig. 1. Relation between z_0, L_{mo} and Turner classes [4].

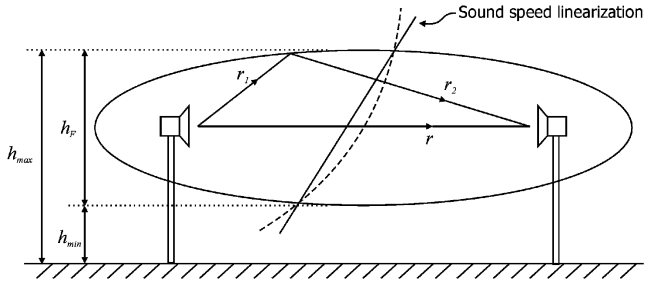

Fig. 3. Fresnel ellipsoid.

From this figure, the constant gradient can be expressed as:

$$g = \frac{s(h_{\max}) - s(h_{\min})}{h_{\mathrm{F}}}, \tag{7}$$

where h_{F} represents the ellipsoid height, that depends both on the wavelength λ and on the emitter–receiver distance r as:

$$h_{\mathrm{F}} = \sqrt{\frac{\lambda}{4} \cdot \left(r + \frac{\lambda}{4}\right)}. \tag{8}$$

2.3. Computation algorithm

The evaluation of (5) is a tedious task that involves many previous calculations necessary to obtain the constant speed gradient g. All these calculations have been automated by programming an algorithm that obtains the desired angle starting from a set of input parameters. For the sake of clarity, these parameters have been classified into three groups:

System parameters: emitter–receiver distance, emitter height, signal frequency and type of terrain.
Meteorological parameters: wind speed, temperature, cloud cover and dew point.
Spatio-temporal location parameters: geographical coordinates of the site, date and time.

Fig. 4 is an schematic representation of the steps followed by this algorithm to perform all the computations. As can be seen in this figure, in the first stage the algorithm calculates three new magnitudes:

(1) The size of the Fresnel ellipsoid, from the input parameters emitter–receiver distance, frequency and emitter height.
(2) The cloud cover height, from the input parameters temperature and dew point which can be more easily measured experimentally.
(3) The solar height, from the input parameters geographical coordinates, date and time.

Next, the algorithm obtains the Turner class from the input parameters wind speed and grade of cloudiness, and from the cloud cover height and solar height calculated in

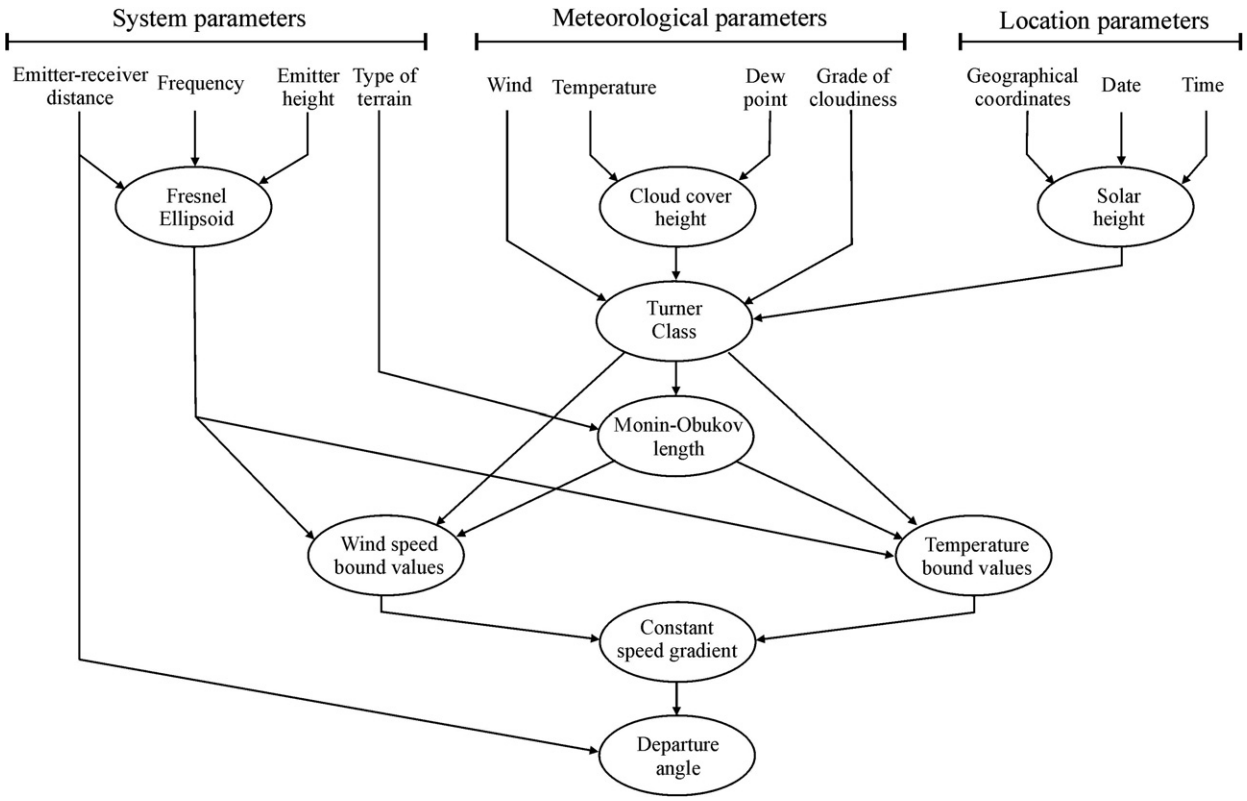

Fig. 4. Computations performed by the developed algorithm.

the first stage. This calculation is based on the algorithm used in [3] to calculate the net radiation index. In the third stage, the algorithm calculates the Monin–Obukhov length from the input parameter type of terrain (roughness length) and the Turner class. This calculation is based on the relation between these magnitudes shown in Fig. 1. For known values of z_0 and the Turner class, the inverse of L_{mo} is obtained as the average between the border values of this magnitude in the corresponding class for the fixed value of z_0.

From the Monin–Obukhov length, the Turner class and the size of the Fresnel ellipsoid, the algorithm calculates the values of temperature and wind speed in the lower and upper extremes of this ellipsoid making use of (3) and (4). Finally, the constant gradient of the apparent sound speed is obtained by evaluating (1) in both boundaries of the Fresnel ellipsoid and then using (7). The departure angle is finally calculated through (5) taking into account the emitter–receiver distance.

3. Pulse compression of refracted emissions

As stated in the introduction, signal coding and pulse compression techniques used in radar theory were introduced in airborne sonars in the nineties, in the field of mobile robotics [7,8]. Since then, these systems have been in continuous evolution and many codes and new signal processing techniques have been proposed to improve their basic capabilities as well as to incorporate new ones.

Signal detection in pulse compression systems is based on the recognition of a certain waveform through correlation with a known pattern. The main advantage of this technique is that the signal-to-noise ratio at the output of the detector can be enhanced by increasing the length but not the amplitude of the emitted signal, and thus, it is not necessary to increase the emitted power to assure the detection of signals in noisy environments. Moreover, since the arrival of the signal is determined by a single pulse that collects all the emitted energy, and not by the envelope of the signal as in the case of a classical system, temporal precision is notably improved. Also, pulse compression allows the detection of two signals received overlapped, since two different pulses are generated after correlation. This implies a significant improvement in the spatial resolution with respect to systems based on threshold detection of the signal envelope.

Nevertheless, signal detection by pulse compression is much more sensitive to all these phenomena that can cause the distortion of the emitted waveforms, like atmospheric refraction analyzed in the previous section. Every ultrasonic transducer is characterized by a particular emission pattern $D(\varphi,\theta)$, showing the dependence of the acoustic pressure field on the direction. Fig. 5 shows the emission pattern of a typical piston-shaped transducer, that can be expressed as follows:

$$D(\varphi,\theta) = D(\theta) = \frac{2J_1(k\cdot a\sin\theta)}{k\cdot a\sin\theta}, \tag{9}$$

where a is the radius of the piston; $k = 2\pi/\lambda$ is the wavenumber; θ is the angle respect to the acoustic axis; and J_1 is the first order Bessel function of the first kind. Fig. 5 shows the particular case of a Polaroid series 600 transducer where $a = 1.7$ cm [9], assuming $T = 20$ °C and $f = 50$ kHz. As can be seen, the emission pattern presents four notches at the angles $\theta = 14.27°$, 26.83°, 40.87° and 58.98°.

Eq. (9) admits another interpretation that is very useful for our purposes. For a fixed angle θ, it gives the response of the transducer as a function of the wavenumber k, or equivalently, it represents the frequency response of the transducer in a given direction. It is easy to see from this expression that, for any angle different from $\theta = 0°$ (propagation along the acoustic axis), D is a function of k and the transducer behaves as a filter of the emitted signal. Depending on the severity of this filtering, an encoded signal leaving with this angle of departure could be so distorted as to be completely unrecognizable by its matched correlator.

This situation is depicted in Fig. 6, where the emission of a 13-bit Barker code through a Polaroid electrostatic trans-

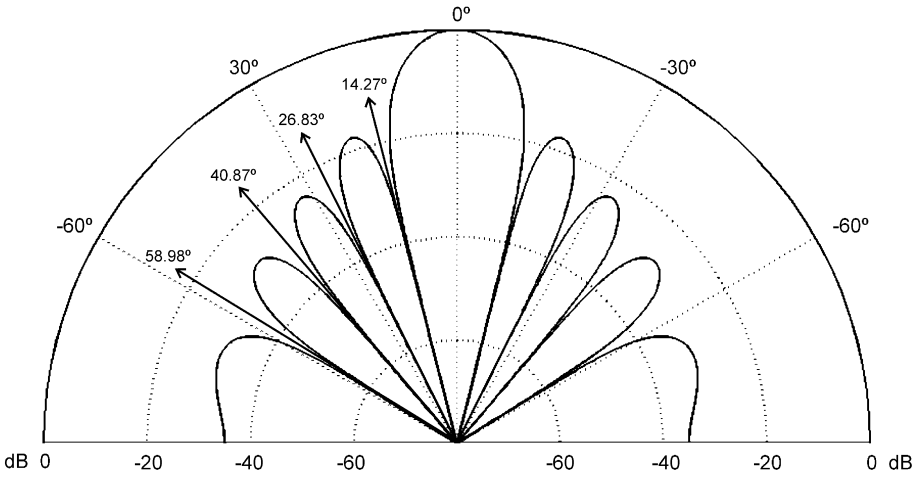

Fig. 5. Emission pattern of the Polaroid transducer for $f = 50$ kHz and $T = 20$ °C.

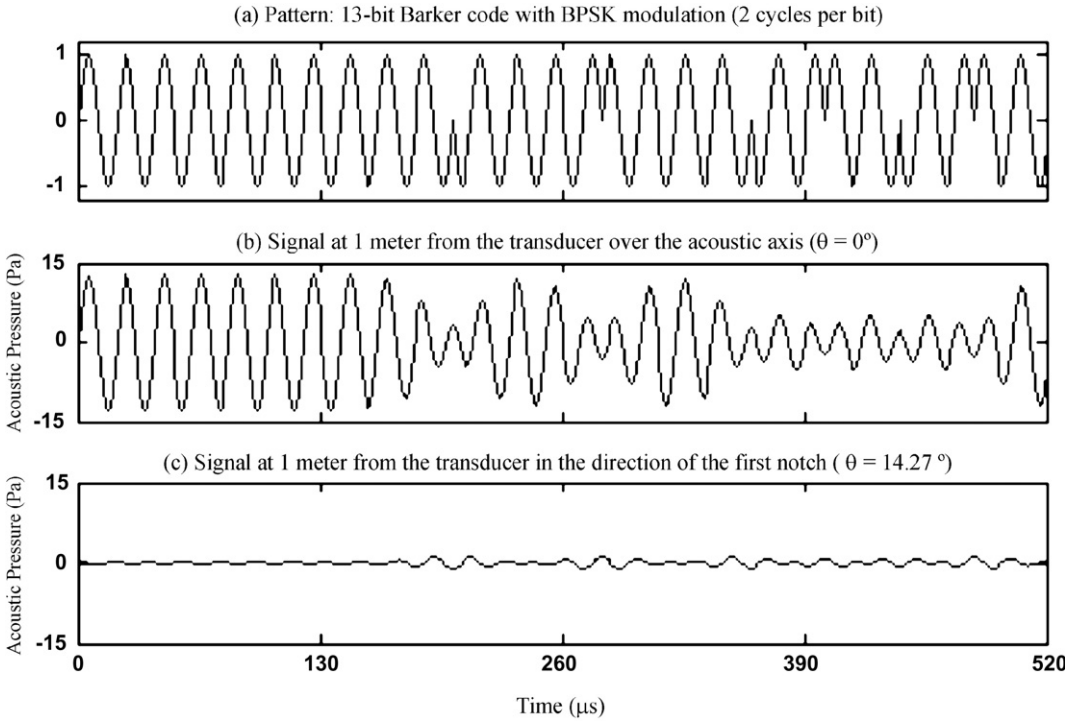

Fig. 6. Filtering effect of the Polaroid transducer in two different directions.

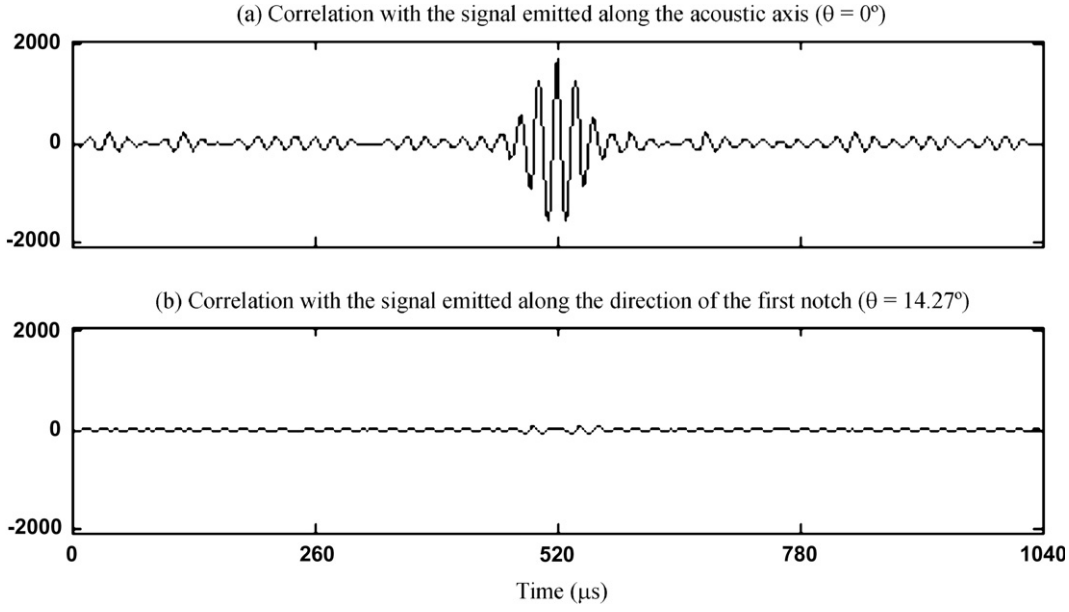

Fig. 7. Correlation of the pattern with the emitted signals.

ducer has been simulated for two different angles. This code has been BPSK[1] modulated with a symbol of two cycles of a 50 kHz ultrasonic carrier, adjusting the spectrum of the emission to the bandwidth of the transducer.

Fig. 6a shows the ideally modulated code before being transmitted, and Fig. 6b and c show the signal emitted at the angles $\theta = 0°$ and 14.27°, respectively. Since the Polaroid transducer is characterized by a radius of $a = 1.7$ cm, this last angle corresponds to the first notch in the emission pattern at the frequency of the carrier ($f = 50$ kHz) for a temperature $T = 20$ °C – see Fig. 5. In this case, the filtering effect is maximum and the signal is notably distorted with respect to the one emitted along the acoustic axis. The consequences of this distortion on the performance of the pulse compressor system are evident in Fig. 7, where it has been represented the correlation of signals from Fig. 6b and c with the pattern in 6a.

[1] Binary Phase-Shift Keying.

After some simulations covering all the angles between 0° and 90° in increments of 1°, it was confirmed that only in the immediate neighbourhood of the notches the filtering is so severe that the emitted signals cannot be properly detected by correlation, a fact first observed in [10]. It can be stated then that atmospheric refraction can have a considerable effect on the performance of an ultrasonic pulse compression system whenever the departure angle of the signal received by the detector is close to a notch in the emission pattern of the transducer at the carrier frequency.

4. Results derived from the study of a particular system

The algorithm presented in Section 2.3 has been used to study the influence of atmospheric refraction on the performance of a real system for outdoor applications that has been recently proposed by the authors [11].

This system is composed of a Polaroid transducer [9] placed at 1.5 m over the ground as the emitter, and a high frequency microphone placed at 14 m from the emitter in the same horizontal plane, as the receiver. This microphone has a reception pattern broad enough as to ignore its filtering effect on the received signal, and thus, it can be assumed that the only distortion of the signal comes from the emitter. The system has been installed over a terrain of short grass ($z_0 = 1$ cm) in a place of geographical coordinates latitude = 30° 47′ N, longitude = 6° 15′ W.

Let us investigate first the effect of temperature-induced refraction. The larger differences of temperature between the ground and the air layers close to it occur at the end of a calm clear night, when the ground has been cooling by radiation and the higher density of cool air reinforce the positive gradient of temperature. In a cold night, with no wind and no clouds, the difference of temperature between the heights of 5 cm and 150 cm above the ground – this last called thermal shield temperature by meteorologists – can be as large as 3–4 °C. According to [3], these meteorological conditions corresponds to a Turner class of 7, and thus from Fig. 1 our algorithm predicts a value of $[0.0572 + (0.1 - 0.0572)/2]^{-1} = 12.72$ m for the Monin–Obukhov length. A value of 0.2861 °C was obtained for the scale parameter T^* assuming temperatures of 1 °C and 5 °C at the heights of 1 cm and 150 cm respectively. The values of these parameters lead to a constant speed gradient of 0.450 ms^{-1}/m that translates into a departure angle of 0.54° for the signal received by the microphone placed at 14 m from the emitter. This angle is well into the main lobe of the Polaroid emission pattern, and thus, no effect is observed in the receiver. Obviously, this situation could get worse with a wind blowing in the direction of propagation, but in this case mechanical turbulence would attenuate the thermal gradient. On the other hand, in a sunny summer afternoon it is possible to find a strong negative gradient of temperature near the ground, but this gradient is never in magnitude as large as the positive one considered before, since the rising tendency of warm air – thermal convection – attenuates the intensity of the thermal gradient.

Let us focus now on the effects of wind-induced refraction. After six months of measurements, comprising from November 2004 to April 2005, the largest value of wind speed registered in this place at the height of 150 cm was 7.8 m/s. Regardless the grade of cloudiness and the cloud cover height, this wind always corresponds to a Turner class of 4, since the solar height never exceeds 60° in the period of the year previously referred.[2] In this case, the algorithm predicts a Monin–Obukhov length of $[-0.0235 + (0.0064 + 0.0235)/2]^{-1} = -116.96$ m, and a value of 0.6227 m/s for the scale parameter v^*. Assuming a practically negligible temperature gradient, a constant speed gradient of 1.0333 ms^{-1}/m and a departure angle of 1.2° are obtained when a wind of this magnitude blows in the direction of propagation. A similar angle but with negative sign corresponds to a wind blowing in the opposite direction. With these wind velocities, it would be necessary to separate the microphone 165 m from the emitter in order to have a departure angle close to the first notch of the emission pattern. In this case, the total attenuation due to geometrical spreading and atmospheric absorption is so high that the only way to detect the signal after matched filtering is through the emission of longer codes. But then, the effect of atmospheric turbulence on the phase of the modulated signal would be even worse than the filtering associated to the emission pattern, as it has been recently observed by the authors in [11].

In order to verify these results experimentally, the continuous emission of a 50 kHz ultrasonic carrier has been conducted under different conditions of wind parallel to the direction of propagation. The main objective of this analysis is to determine whether the presence of wind causes significant differences between the experimentally measured attenuation A_{exp} and the theoretical one A_{th}, this last one obtained as the sum of the geometrical spreading attenuation A_{gs} and the atmospheric absorption A_{abs}, i.e.,

$$A_{\mathrm{th}} = A_{\mathrm{gs}} + A_{\mathrm{abs}} = 20\log r + 8.67\alpha_{\mathrm{a}} r \quad (\mathrm{dB}), \tag{10}$$

where r is the traveling distance and α_{a} represents the absorption coefficient, a function of frequency, temperature, humidity and pressure that can be easily obtained through the formulation presented in [12].

The amplitude of the received tone has been accurately measured by sampling this signal at a rate of 800 kHz and then digitally filtering these samples to remove the presence of undesired signals. Next, the energy contained in every set of 16 consecutive samples has been calculated to obtain a measure of the instantaneous amplitude as one-eighth the square root of this energy. All the measurements have been conducted under solar height and cloud cover conditions corresponding to neutral atmospheres (Turner class of 4), thus minimizing the effects of temperature-induced refraction. Different values of temperature T and humidity H have been considered during the experi-

[2] Actually, this limit is surpassed for a few minutes the last days of April.

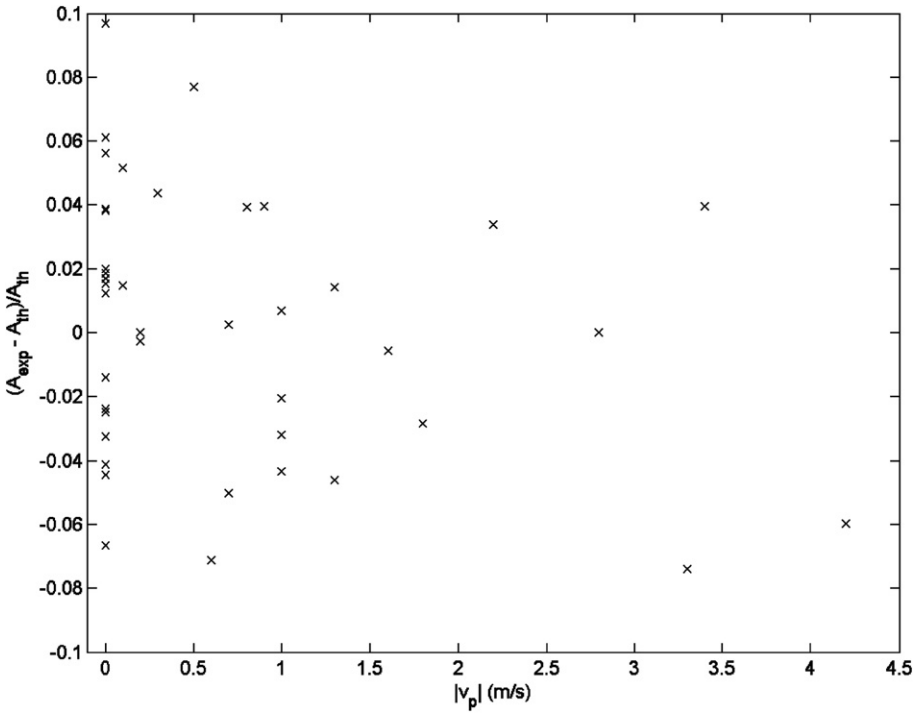

Fig. 8. Relative differences between the theoretical A_{th} and the experimental A_{exp} attenuations as a function of the parallel component of wind v_p.

mentation, with theoretical values of atmospheric absorption ranging from 0.870 dB/m ($T = 6°$ and $H = 56\%$) to 1.497 dB/m ($T = 12°$ and $H = 86\%$).

The results of this analysis are represented in Fig. 8, where it can be seen that the relative differences between the experimental and the theoretical attenuation never exceed 10%, and also, and more important, that there is no apparent correlation between these differences and the magnitude of the parallel wind, a fact that confirms the negligible effect of atmospheric refraction on the system under analysis.

5. Conclusions

In this paper the effect of atmospheric refraction on the performance of an ultrasonic pulse compression system has been addressed. First, this phenomenon has been thoroughly studied to obtain a general formulation that allows the calculation of the departure angle of an horizontally emitted ray depending on the particular meteorological conditions. Since the obtaining of this angle involves many previous calculations, a computation algorithm has been proposed to automate all the process, and the structure of this algorithm has been described.

Second, the influence of the departure angle of an ultrasonic ray on the detection of the encoded signal by matched filtering has been analysed assuming the emission of a 13-bit Baker code BPSK modulated through a Polaroid electrostatic transducer. It has been seen that the detection of these signals could fail whenever the departure angle is close to a notch in the emission pattern of the transducer.

Next, a real system has been experimentally and theoretically studied making use of the algorithm previously devised. The main conclusion that can be drawn from the results of these studies is that atmospheric refraction seems not to have a significant influence on the performance of an ultrasonic pulse compression system provided the emission pattern of the transducers is wide enough, this width depending on the maximum desired range of operation and the maximum wind speed expected at the height of the emitter. In most practical situations, with maximum ranges of operation of several tens of meters and maximum wind speeds of about 8 m/s at the emitter height, the first notch of the emission pattern is always far from the critical departure angle.

Finally, it is important to remark that the main advantage of the algorithm presented in this paper is its parameterized codification, a feature that allows the analysis of the refraction effects in any other configuration with different values of geographical coordinates, type of terrain, emitter height, maximum range or signal frequency.

References

[1] Cuerva A, Sanz-Andrés A. On sonic anemometer measurement theory. J Wind Eng Ind Aerodyn 2000;88(1):25–55.
[2] Monin AS, Obukhov AM. Basic laws of turbulent mixing in the ground layer of the atmosphere. Trans Geophys Ins. Akad, Nauk USSR 1954;24(151):163–87.
[3] Panofsky HA, Dutton JA. Atmospheric turbulence. In: Models and methods for engineering applications. John Wiley and Sons; 1984.
[4] Golder D. Relations among stability parameters in the surface layer. Boundary-Layer Meteorol 1972;3(1):47–58.

[5] Embleton TF. Tutorial on sound propagation outdoors. J Acoust Soc Am 1996;100(1):31–48.
[6] L'Espérance A, Daigle G. The estimation of the linear sound speed profiles under general meteorological conditions. Can Acoust 1994;22(3):125–6.
[7] Peremans H, Audenaert K, Campenhout JV. A high resolution sensor based on tri-aural perception. IEEE Trans Robot Automat 1993;9:36–48.
[8] Jörg K-W, Berg M. Sophisticated mobile robot sonar sensing with pseudo-random codes. Robot Autonom Syst 1998;25:241–51.
[9] Polaroid Corporation, 600 Series. Instrument Grade Electrostatic Transducers. Technical Specification (January 1999).
[10] Peremans H. Tri-aural perception for mobile robots, PhD thesis, Department of Electronics and Information Systems Belgium: University of Gent, 1994.
[11] Álvarez FJ, Ureña J, Mazo M, Hernández A, García JJ, Marziani CD. High reliability outdoor sonar prototype based on efficient signal coding. IEEE Trans Ultrason, Ferroelectr Frequency Control 2006;53(10):1862–71.
[12] ISO/TC 43 Technical Committee, Acoustics, Sub-Committee SC1, Noise, Attenuation of sound during propagation outdoors. Part 1: Calculation of the absorption of sound by the atmosphere, Tech. Rep. ISO 9613-1:1993(E), International Organization for Standarization (1993).